# Demonstration of 3-dimensional wide-angle no-moving-parts laser beam steering

Khan, Sajjad, Riza, Nabeel

Sajjad A. Khan, Nabeel A. Riza, "Demonstration of 3-dimensional wide-angle no-moving-parts laser beam steering," Proc. SPIE 5550, Free-Space Laser Communications IV, (20 October 2004); doi: 10.1117/12.561810

SPIE.

Event: Optical Science and Technology, the SPIE 49th Annual Meeting, 2004, Denver, Colorado, United States

# Demonstration of 3-Dimensional Wide Angle No-Moving Parts Laser Beam Steering

Sajjad A. Khan and Nabeel A. Riza

Photonic Information Processing Systems Laboratory
College of Optics and Photonics/Center for Research and Education in Optics and Lasers (CREOL)
University of Central Florida, 4000 Central Florida Blvd., Orlando, FL 32816-2700
Tel: 407-823-6829; Fax: 407-823-6880; E-mail: nriza@mail.ucf.edu

## Abstract

Design and demonstration of a versatile liquid crystal-based scanner is shown for steering a laser beam in three dimensions. The scanner consists of a unique combination of digital and analog control polarization-based beamforming optics resulting in both continuous and random fashion beam steering. The scanner features a novel device biasing method, large aperture beamforming optics, low electrical power consumption, and ultra-fine as well as wide angle coarse beam steering. Demonstrations include one, two and three dimensional beam steering with a maximum of $40.92^{o}$ continuous scan, all at 1550 nm. The minimum scanner aperture is 1 cm diameter and uses a combination of ferroelectric and nematic liquid crystals in addition to Rutile crystal birefringent prisms.

**Keywords**: Optical communications, Polarization-sensitive devices, Optical Scanners, Liquid crystals.

## 1. Introduction

An optical scanner is a device that can control the position of a light beam in one or more orthogonal spatial dimensions. As early as the 1960s, researchers have proposed and demonstrated several techniques with varying success that can be used to scan a laser beam. These include scanners based on birefringent crystals,[1-9] nematic liquid crystals (NLCs),[10] ferroelectric liquid crystals (FLCs),[11] optical microelectromechanical systems (MEMS),[12] and ferroelectric electrooptic materials such as lead zirconate titanate.[13,14] Several applications can benefit from 3-D beam steering where a beam of light can be translated in two orthogonal spatial directions transverse to the beam propagation direction as well as be focused/defocused along the propagation direction. The focusing ability is highly desirable in applications where the received information-carrying beam is to be focused on a small detector area, as it will improve the signal-to-noise ratio and hence decrease the probability of error in the received signal. A number of polarization based scanners have been demonstrated which use the property of birefringent media to steer the optical beam in two different directions based upon the state of polarization of the incident light.[15-20] A polarization switch is used to control the state of polarization of the light while a passive birefringent material prism is used to steer the beam into one of the two scanning destinations. By cascading several polarization switch-prism pairs, multiple scan spots can be obtained. The birefringent material prisms used so far have been passive devices whereby the linearly polarized beam incident upon them will generate one of the two fixed spots based upon the state of linear polarization of the incident beam. Apart from birefringent crystals,[1-9,15] these passive birefringent devices have included liquid crystal (LC) filled prisms (i.e., the LC cell enclosure is shaped like a glass prism).[16,17] This fixed LC prism approach is effective for small (e.g., a few degrees) angular deflections as the preferred molecular orientation of the LC molecules can not be preserved in thicker high birefringence LC cells, leading to increased scattering losses. These previously demonstrated polarization based scanners (Refs. [1-9,15-17]) have been limited to 1-D and 2-D scans with discrete scan beam spots. Other limitations of these scanners have included high drive voltages, pixelation, and non-programmable birefringent plate designs.

In certain applications it is desirable to have the ability to quickly reconfigure the scan directions to cover for errors in the overall scanning system. Such example applications are free-space optical wireless, inter-satellites



Free-Space Laser Communications IV, edited by Jennifer C. Ricklin, David G. Voelz, Proceedings of SPIE Vol. 5550 (SPIE, Bellingham, WA, 2004)
0277-786X/04/$15 doi: 10.1117/12.561810

links, optical microscopy, mobile military platforms, and 3-D displays. For example in free-space optical wireless links, reconfigurability is needed to counter for building sways or temperature and weather fluctuations that cause a variation in the index of the air medium and hence a change in the direction of the outgoing optical beam from the scanning device. In another case, inter-satellite links need fine angular scanning tunability of the order of 1μrad at high speeds (e.g., 1 KHz)[21] to keep track of the fast moving destination satellite.[22] Yet another case of mobile military platforms needs a scan dynamic range of ±45°.[23] Hence, demand exists for a no moving parts, 3-D scanner that can provide both random and continuously addressable scanning over a large angular scan dynamic range with high resolution beam control.

Recently, such a 3-D scanner was proposed that can continuously scan a large angular dynamic range and has the capability to address the third dimension; i.e., the ability to focus or defocus a beam of light along its direction of propagation.[18] The demonstration showed how large aperture, non-pixelated liquid crystal devices can be used to form a fully programmable high speed polarization based scanner.[19] In this paper, the ref. 19 concept is extended to demonstrate a 3-D Polarization-Multiplexed Optical Scanner (P-MOS) for random as well as continuous optical scanning over a wide angular dynamic range while maintaining high resolution beam pointing control.[20] Specifically, multiple proof-of-concept experiments at the telecommunications band wavelength of 1550 nm are carried out and results are presented. Video demonstrations of these experiments (Figs. 3,5,7,9 and 10) can be found in ref#20 and the Optics Express website.
http://www.opticsexpress.org/abstract.cfm?URI=OPEX-12-5-868

## 2. Hybrid analog-digital P-MOS design

In the proposed hybrid analog-digital P-MOS, the state-of-polarization of a linearly polarized incident laser beam is controlled in orthogonal states to achieve beam scanning. As shown in Fig. 1, key elements of the proposed P-MOS are a polarization control element and a polarization dependent beam steering element. For polarization control, fast response digitally controlled 90° polarization switches (PSs) are used. For angular scanning, birefringent material prisms (Ws) are used to steer the beam into a desired spot. Using N polarization switch-prism pairs $2^N$ scan spots can be obtained. For coarse angular scanning, passive birefringent crystal prisms are used. Multiple coarse stages are cascaded to achieve a large angular dynamic range with discrete scan spots. To fill the uncovered spaces between these discrete scan spots, analog-mode electrically controlled NLC prisms are incorporated into the scanner design to realize a true analog-digital hybrid controls scanner. The Fig. 1 design shows a P-MOS capable of continuous 1-D scanning where the NLC device acts as an analog control programmable varying tilt prism. Specifically, by switching the electrode drive signal of the NLC device, the tilt direction can be flipped, thus leading to an effective doubling of the NLC prism effect by using just one NLC tilt prism. As later explained in detail, this idea is key to the design of the proposed P-MOS that can allow a high resolution beam scan between the discrete states of the P-MOS.

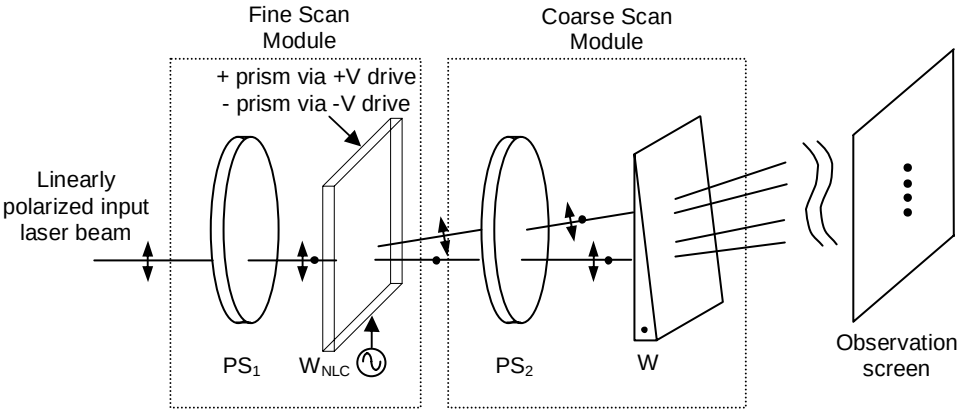


Fig. 1. Design of the proposed hybrid analog-digital coarse-fine scan P-MOS module for continuous 1-D scanning. PS: 90° Polarization Switch, W: Passive Crystal Prism; $W_{NLC}$; Nematic Liquid Crystal Electrically Programmable Prism set for a given drive voltage. Shown are four possible 1-D scan beams produced by digital only switching of the PSs.

Recall that in the P-MOS, one PS and one prism combine to form one deflection stage. Moreover, two such 1-D stages can be cascaded in the orthogonal orientation to achieve a 2-D scanner. As opposed to scanners that use pixelated elements for beam scanning where some power is coupled into higher diffraction orders resulting in lower throughput efficiency, the proposed P-MOS design utilizes large-aperture pixel-free devices resulting in diffraction order free beam steering.

LC based devices have also been used to demonstrate focusing/defocusing of laser beams.[18-21,30,32] Due to their birefringent nature, these devices work for only one polarization. If the input light polarization is parallel to the LC molecular director, the light gets focused/defocused; otherwise it passes through the LC cell un-perturbed. Hence, these LC based lenses can be effectively used in 3-D P-MOS scanning.

In order to manipulate the laser beam position at a desired point in space, the linear polarization of the incident beam is controlled using for example, electrically switchable FLC half-wave plates. FLC polarization switches are used because of their fast switching speed (several microseconds), low voltage (e.g., ±5 V) digital operation, and thin cell design. Specifically, 90° polarization rotation is achieved by re-orientation of the FLC director due to Clarke-Lagerwall effect induced by the application of a bipolar electric field across the cell.[24] The retardation for an FLC birefringent phase plate can be expressed by the relation:

$$\Gamma = 2\pi \, \Delta n \, . \, d/\lambda \tag{1}$$

where $\Delta n$ is the birefringence of the FLC material and d is the FLC cell thickness. For a given wavelength and FLC material, the thickness of the half wave plate is given as:

$$d = (\lambda \, . \, \Delta n) \, /2 \tag{2}$$

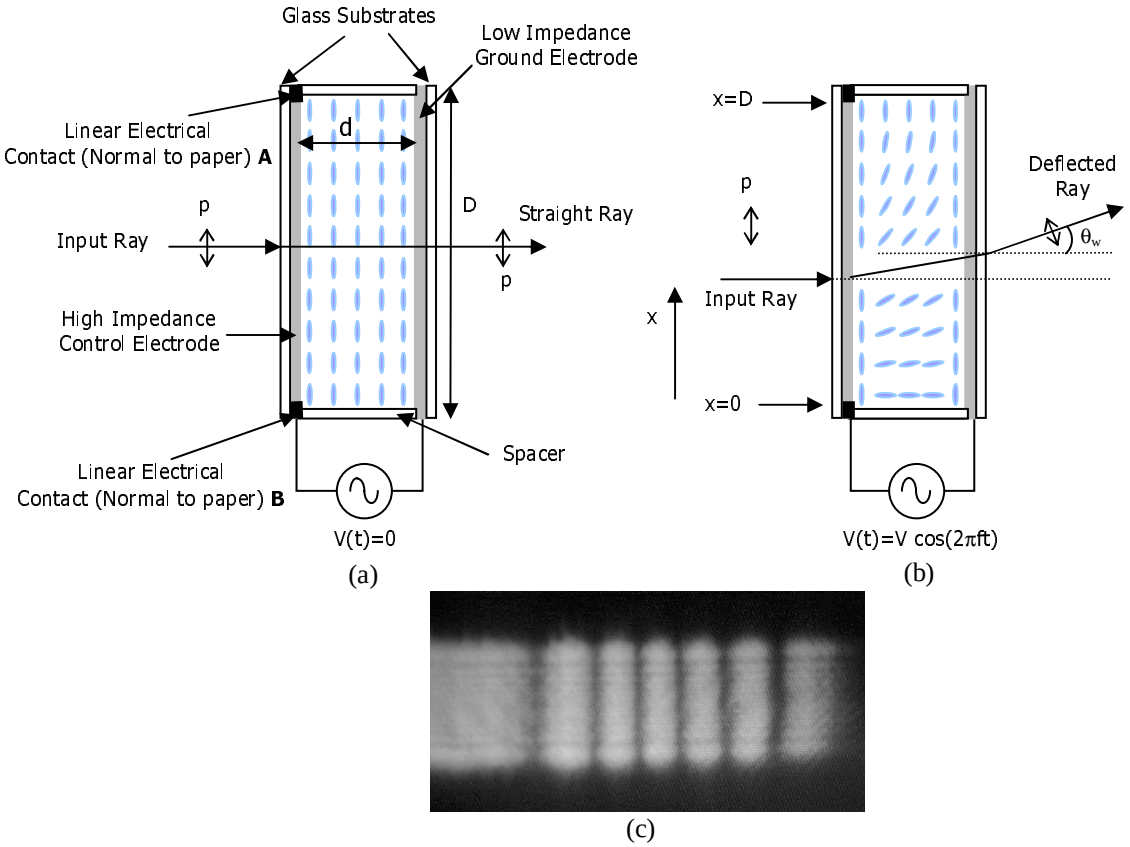


Fig. 2. Top views of the NLC prism used for continuous scan in P-MOS. NLC molecule orientations are shown for (a) no control signal applied, (b) when a control signal is present that reorients the NLC molecules to induce a spatial prism-like refractive index change and (c) the interferogram of the NLC prism using a 1550 nm source. p: horizontally polarized light component.

For $\lambda$=1550 nm, the FLC material has a birefringence of 0.14 ($\Delta n=n_e-n_o$=1.62-1.48), giving a half-wave plate thickness of 5.54 $\mu$m.[25] Thus a thin FLC cell is formed for effective cascading with the P-MOS design.

For the P-MOS, the NLC prism device is a homogeneously aligned NLC cell with uniform thickness.[26-27] The design is slightly different from an ordinary NLC cell in that the glass substrates are deposited with two different electrodes. One substrate is deposited with a low impedance layer such as Indium Tin Oxide (ITO) for use as the ground electrode while the other substrate is deposited with a uniform layer of high impedance material for use as the control electrode. To use these NLC cells as angular deflectors, voltage is applied between two parallel linear metallic contacts that are deposited at the edges of the control electrode. This results in a linearly varying electric field between the front (control) and back (ground) electrodes causing the index to vary in a near linear fashion across the clear aperture of the device. This index modulation can only be seen by that component of the input polarization which is along the director of the liquid crystal. As shown in Fig. 2, a ray polarized along the molecular NLC director passing through the NLC prism acquires a phase shift at the device position x that can be expressed as:

$$\phi(V, f, x) = [2\pi/\lambda]\, n(V, f, x)\, .\, d \tag{3}$$

where $\lambda$ is the optical wavelength, d is the NLC layer thickness, n(V, f, x) is the electrically controlled NLC refractive index the light sees, and V is the amplitude in Volts and f is the frequency in Hertz of the NLC device drive signal. Looking at the two extreme ray positions of x=0 and x=D, the beam deflection of the entire wavefront incident on the NLC prism can be studied. Specifically, the x=0 position ray suffers a phase shift given by:

$$\phi(V, f, x=0) = \phi_o = [2\pi/\lambda]\, n(V, f, 0)\, .\, d\,, \tag{4}$$

while the extreme ray at x=D suffers a phase shift given by:

$$\phi(V, f, x=D) = \phi_D = [2\pi/\lambda]\, n(V, f, D)\, .\, d\,. \tag{5}$$

Hence the phase shift between the edges of refracted plane wave exiting the NLC prism is given by:

$$\Delta\phi_A=\phi_D-\phi_o\,, \tag{6}$$

where between the x=0 and x=D points, the incident plane wave acquires a linearly increasing phase shift. For state A of the NLC deflector, at x=D, the applied voltage is below a certain threshold level, so the index seen by the incoming ray of *p*-polarization is essentially $n_e$, the NLC material extraordinary index of refraction. Therefore $\phi_D = 2\pi/\lambda\, .\, (n_e\, .\, d)$ and $\Delta\phi_A$ becomes:

$$\Delta\phi_A = (2\pi/\lambda)\, [n_e-n(V, f, 0)]\, d\,. \tag{7}$$

Similarly, note that at the x=0 location where the other device electrode is present in state A, V and f can be controlled to set $n(V, f, x=0) = n_o$, where $n_o$ is the ordinary refractive index of the NLC material. In this case, the prism is generating its maximum birefringence $\Delta n = n_e-n_o$ and hence also produces the largest phase shift between rays across the device aperture D. This in turn leads to the maximum beam deflection angle $\theta_m$ for the programmable NLC prism. From phased array theory, the beam steered angle $\theta_{w_1}$ due to an inter-element phase shift $\Delta\phi_A$ is given by:

$$(2\pi D/\lambda)\, \sin\theta_{w_1} = \Delta\phi_A, \tag{8}$$

where D is the phased array inter-element distance or in this case the NLC prism aperture. By equating equations (7) and (8), the electrically controlled prism angle $\theta_{w_1}$ as seen by a wave polarized along the molecular director is written as:

$$(2\pi D/\lambda)\, \sin\theta_{w_1} = (2\pi/\lambda)\, [n_e-n(V, f)]\, .\, d \tag{9}$$

This in turn leads to:

$$\theta_{w_1}(V, f) = \sin^{-1}\{\frac{d}{D}\, [n_e-n(V, f)]\}, \tag{10}$$

Since $\theta_{w_1}$ is a function of the control signal amplitude and frequency, the output can be steered in different directions by controlling the drive signal. This results in an actively reconfigurable prism where the prism apex angle and hence the steering beam direction can be programmed as per demand.

A critical aspect of this NLC deflector device is exploited in the design of the proposed P-MOS; namely, the switching of the drive signals to the two control electrodes on the high impedance substrate of the cell. In effect, for state B of the NLC device,

$$\Delta\phi_B=\phi_D-\phi_o\ , \tag{11}$$

$$\Delta\phi_B = (2\pi/\lambda)\ [n(V, f, D)- n_e] \ .\ d \tag{12}$$

$$\Delta\phi_B = -\Delta\phi_A \tag{13}$$

Hence, equation (13) implies that in state B of the NLC deflector, the tilt direction is reversed and the tilt angle $\theta_{w_2} = -\ \theta_{w_1} = \theta_w$. In short, an input laser beam can be made to sweep a symmetric positive and negative angle $\theta_w$ about the laser beam input axis. Using electrical drive switching, thus, the given single NLC deflector device with a fixed maximum birefringence $n_e$-$n_o$ can be used to produce double the tilt control as compared to the non-switched NLC deflector device. This specific benefit is exploited in the proposed P-MOS to enable a near continuous beam scan field.

In order to get scanning in the longitudinal direction (along the beam propagation direction), any NLC based lens can be used. The structure of the used NLC lens is very similar to that of the NLC deflector, except for an annular electrical contact that is deposited on the periphery of the device aperture instead of the linear contacts for the deflector. When the control signal is applied across the NLC lens cell using this annular contact, the voltage drops from the edge to the center of the clear aperture in a quadratic fashion. The consequence of this voltage variation is a lens-like index distribution between the front and back electrode of the device that can be seen only by the input light polarization which is parallel to the NLC molecular director. For an NLC lens with a clear aperture of diameter D and a cell thickness of d, the focal length F using the Fresnel's approximation is given by:[26]

$$F = \frac{D^2}{8d\left(\Delta n_c - \Delta n_p\right)}\ , \tag{14}$$

where $\Delta n_c$ and $\Delta n_p$ are the birefringences at the center of the NLC lens cell and the periphery of the annular contact, respectively. Since, $\Delta n_c$ and $\Delta n_p$ are a function of the drive voltage and frequency, therefore the focal length F can be varied by varying the control signal. Moreover, the difference of these two can be made equal to the intrinsic birefringence $\Delta n$ by controlling the drive signal. So, for an NLC lens cell with 50 μm cell thickness and 5 mm clear aperture diameter, the focal length F using Merck BL006 ($\Delta n$=0.229) is 27.3 cm at $\lambda$=1550 nm. Notice that F will be different for different wavelengths following the birefringence dispersion of the NLC material used. By changing the amplitude and frequency of the applied signal, the lens power can be varied in a desired fashion to focus the laser beam at a desired spot along the propagation direction. Use of these NLC lenses with the earlier described deflectors can result in realizing 3-D beam scanning.

As mentioned earlier, in order to get large angular deflections, the P-MOS also uses fixed birefringent crystal prisms. The optic axis (c-axis) of the birefringent crystal prism can be oriented such that the *s* and *p* polarizations each experience a different index of refraction. At the entrance face the following relation holds true:

$$n_{inc} \sin\theta_{inc} = n_o \sin\theta_o = n_e \sin\theta_e\ , \tag{15}$$

where $n_{inc}$ is the index of refraction of the material surrounding the birefringent crystal prism, $\theta_{inc}$ is the angle of incidence with respect to the normal to the prism entrance surface, and $\theta_o$ and $\theta_e$ are the refracted angles inside the birefringent material as seen by the ordinary $n_o$ and extra-ordinary $n_e$ indices, respectively. At the exit face we have:

$$\theta_{exit[o]} = \sin^{-1}[n_o \sin(\theta_o+\alpha)/n_{inc}\ ] - (\alpha+\theta_{inc}) \tag{16}$$

$$\theta_{exit[e]} = \sin^{-1}[n_e \sin(\theta_e+\alpha)/n_{inc}\ ] - (\alpha+\theta_{inc})\ , \tag{17}$$

where $\alpha$ is the apex angle of the prism and $\theta_{exit}$ is measured from the incident beam direction. In the case when $n_{inc}$ =1 and the first prism (in a cascade of such birefringent crystal prisms) interface is normal to the incident light propagation direction, $\theta_{inc}$ = 0, equations (16) and (17) reduce to:

$$\theta_{exit[o]} = \sin^{-1}[n_o \sin(\alpha)] - \alpha \tag{18}$$

$$\theta_{exit[e]} = \sin^{-1}[n_e \sin(\alpha)] - \alpha \tag{19}$$

$$\Delta\theta = \theta_{exit[e]} - \theta_{exit[o]}\ . \tag{20}$$

Successive application of the boundary conditions gives the exit angles from a birefringent crystal prism. As seen from equations (16-20), the angular separation, $\Delta\theta$, between the ordinary and the extra-ordinary components of the light emerging from the prism depends upon the angle of incidence, the two indices and the apex angle of the prism. For large index or large apex angle the angular separation is larger. Also, higher birefringence will result in larger separation. Another important point to note is that two different materials with the same value for birefringence $\Delta n$ but with different average index will result in different values for angular separation where we assume the same apex and incidence angles. Although large index of refraction is desirable as it results in thinner angular prisms, these prisms must be carefully coated with anti-reflection layers to reduce Fresnel reflections from the prism surfaces. Fresnel reflections are an important aspect to consider in a cascaded design as they can cause high insertion losses for the proposed scanner. Moreover, one needs to make sure that the absorption coefficient of the material is small in the wavelength band of operation of the P-MOS.

## 3. Experiments

The goals of the P-MOS experiment are to demonstrate large angular scans as well as 3-D scans in both random and continuous fashion. Multiple experiments were conducted to demonstrate beam deflection in one, two and three dimensions. All the experiments were conducted at the telecommunications band wavelength of 1550 nm using a 0.5 mm $1/e^2$ diameter collimated beam from a fiber coupled semiconductor laser. In the first experiment, 1-D beam deflection is demonstrated in digital (random access) fashion where a single birefringent crystal prism made of Rutile ($n_e$=2.454, $n_o$=2.71 @ $\lambda$=1550 nm) and an NLC (Merck BL006, $\Delta n$ =0.229 at 1550 nm and 25$^o$ C) prism are used to scan the beam into $2^2$ = 4 spots. The Rutile prisms have a clear aperture of 2 cm x 2 cm and are anti-reflection (AR) coated. The non-AR coated NLC cell used has a 5 mm aperture and a 50 μm thickness. The configuration used is exactly that of Fig. 1. Two FLC polarization switches are used to control the polarization of the 1550 nm laser beam in digital fashion in order to address these 4 spots. Figure 3 shows the resulting experimentally measured far-field spot pattern for this experimental configuration. The two yellow spots show the birefringent crystal prism deflection spots whereas the white spots are from the NLC prism deflection. Notice that in this demonstration the NLC prism is always turned on with a given fixed voltage/frequency drive and only the beam polarization is controlled to produce the scanning far field spot pattern.

An important aspect of the NLC prism cell is highlighted in Fig. 4(a); namely the bias switching controls for the NLC prism as discussed earlier in Eq. (13). In Fig. 4(b-d), effective NLC cell shape and beam deflections for a two stage P-MOS are shown where one NLC prism and one birefringent crystal prism have been used as outlined in the design of Fig. 1. In Fig. 4 (b), when the drive signal is in the OFF state, the NLC cell acts as an ordinary birefringent material cell, causing a uniform phase retardation throughout the NLC cell aperture. The birefringent

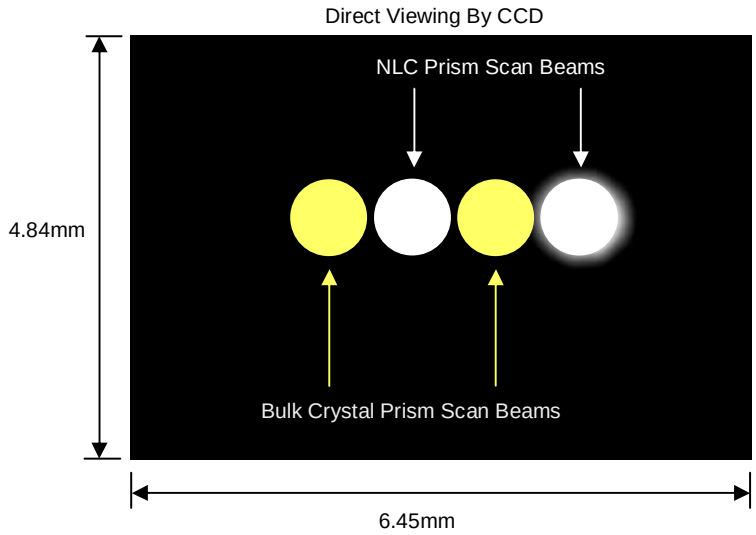


Fig. 3. Experimentally obtained far-field spot pattern for a basic 2-stage 1-D coarse-fine P-MOS demonstration at 1550 nm using only digital addressing.

crystal prism in Fig. 4(b) causes the beam to be steered into two different spots K and L depending upon the polarization of the incoming laser beam. For simplicity, the FLC PSs have not been shown in Fig. 4. In Fig. 4(c), when the switch is thrown to state A (i.e., when $V_A > V_B$), an index ramp is formed across the NLC cell aperture converting it into an effective prism that will deflect the light polarized along the NLC molecular director. This process in-turn causes the two deflections from the birefringent crystal prism to be shifted to the L and M positions and the angular scan to be doubled in the small angle approximation regime (i.e., $\sin\theta \cong \theta$) as compared to the case when only a single birefringent crystal prism is used. Figure 4 (d) shows the case when the switch is set to state B

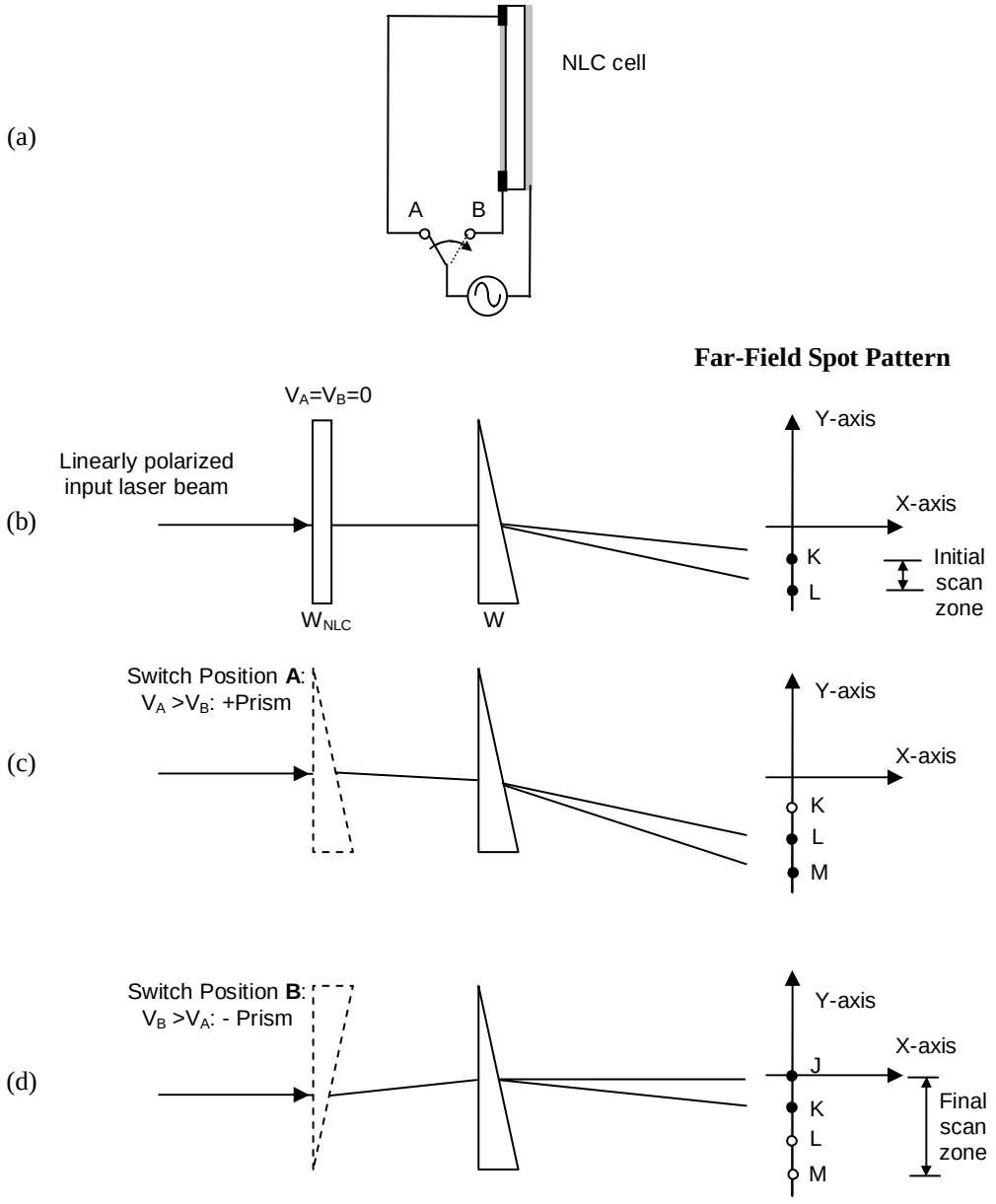


Fig. 4. (a). Proposed Biasing Technique for the NLC prism. Fig. 4(b-d): The effective NLC cell shape and beam deflections for a two stage P-MOS where one NLC prism and one birefringent crystal prism W have been used as shown in Fig. 1. Shown are NLC device states when (b): drive signal is OFF, (c): switch is set to state A (i.e., when $V_A > V_B$), and (d): switch is in state B (i.e., when $V_B > V_A$). Dark spots along the Y-axis represent the far-field spots as produced by the shown NLC device state while the white spots represent the total scan spots possible including those from the alternative NLC device states.

(i.e., when $V_B > V_A$) causing an index ramp in the direction opposite to the previous case, resulting in the output beam from the two stage P-MOS to be steered into positions J and K. These corresponding far-field spots are shown at the right of Figs. 4(b-d). As can be seen from the far-field spot pattern in Fig. 4(d), the scan zone is three times the scan zone when the NLC prism was not used. If instead of the NLC prism device, another birefringent crystal prism is used with the same apex angle, the total scan zone is only doubled and not tripled. In addition, when using the fixed apex angle prisms (such as birefringent crystal prisms or LC filled passive prisms), there is no mechanism for covering the intermediate space between the spots from these prisms. Hence, the unique electrode bias switching not only increases the scan zone, but via NLC device drive signal amplitude and frequency control actively covers the intermediate space between the birefringent crystal prism scan spots (as shown later in, Fig. 7).

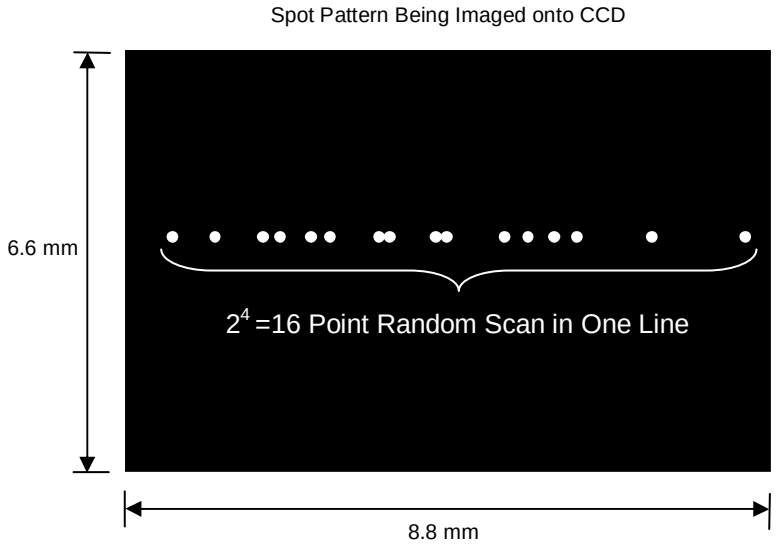


Fig. 5. Experimentally obtained far-field spot pattern for 4-stage 1-D coarse digital P-MOS demonstration at 1550nm. $\alpha_1 = -9.95^o$, $\alpha_2 = 19.95^o$, $\alpha_3 = 4.95^o$ and $\alpha_4 = 9.95^o$ using Rutile prisms ($n_e$=2.454, $n_o$=2.71 @ $\lambda$=1550nm). $\alpha$: apex angle of prism.

In the second experiment, 1-D large angular beam deflection is demonstrated where four birefringent crystal prisms and four FLC polarization switches are used to scan the beam into $2^4 = 16$ spots. The angular scan dynamic range is $33.11^o$ as shown by the star * data-set in Fig. 6 and the video frames captured in Fig. 5. The maximum angular separation between any two spots in this experiment is $7.12^o$ as shown by the difference between polarization states#15 and 16 (see Fig. 6). As noted from equations (16-20), the linear approximation to Snell's law can not be applied for large angles and hence as the deflection angle increases, so does the non-linearity in the angular separation between scan points. In order to cover for such non uniform angular separation of the far field spot pattern, an NLC prism is introduced at the input to the first stage in the P-MOS setup. The NLC device molecular director is oriented along the incident laser beam polarization direction (*p* in this case). Computer based simulation are carried out in order to determine the desired electrically controlled angle of the NLC prism device to completely fill the gaps between the spot pattern. As shown in Fig. 2, since the NLC prism has two linear contacts at the edges of the control electrode marked A and B, one of the contacts is set at the threshold voltage for the NLC cell. At the other contact, a higher voltage is applied such that an index ramp is formed in the NLC cell along, say, +x-dimension which results in a thin optical prism that can be seen by only one polarization component (*p* in this case). Controlling the potential difference between these two metallic contacts results in varying the optical prism apex angle. As mentioned earlier, by swapping the voltage levels between these two contacts, the index ramp and hence the prism angle can be formed along the -x-dimension. The simulation was carried out keeping in mind this dual nature of the given NLC device prism angle. From the conducted simulation, the NLC prism angle $\pm\theta_w$ needed for completely filling this experimental design spot pattern is found out to be $\pm 0.35^o$. The resulting range of angles that can be accessed by this experimental P-MOS scanner are shown in Fig. 6 by the dataset labeled star ☆ and cross + for $-\theta_w$ and $+\theta_w$, respectively. The NLC prisms used had a cell thickness of 50 μm and a clear aperture of 5 mm. The maximum prism angle $\theta_w$ that was obtained from these devices was $0.131^o$, so three of the NLC prism devices were

cascaded to form an equivalent NLC wedge in order to achieve a continuously tunable scan of 0.35°. The experimental scanning demonstration works as follows: All the PSs are controlled such that the scanner output beam corresponds to a certain polarization state#, say, for example 1. The NLC wedge module is driven with voltages that result in $\theta_w$ = -0.35°. The output beam from the scanner corresponds to the initial or starting point for the scan domain. The polarization switches are kept in the same state and the NLC drive signal is varied such that $\theta_w$ decreases gradually from -0.35° to 0° which is also the state corresponding to the spot generated by the bulk crystal prisms in the absence of the NLC prism in polarization state#1. Then the voltage levels between the two metallic contacts A and B are inter-changed so that the NLC index ramp corresponds to a positive angle $+\theta_w$ and the drive signal is varied such that $\theta_w$ increases from 0° to +0.35°. Once, the maximum0.35° has been reached, the control state of the PSs is varied such that they correspond to polarization states#2. Again, the NLC prism angle $\theta_w$ is varied, following the same sequence as in polarization state#1, i.e., from -0.35° to +0.35°. Once the maximum $\theta_w$ is reached, the polarization state can be switched to the next higher level and the same sequence of steps is followed until the whole scan domain is accessed in this manner. It can be noticed from Fig. 6 that in some of the polarization states, the steering angle values overlap with the adjacent polarization states. This means that in order to scan the angular zone corresponding to such a polarization state, scanning will start with an intermediate value of $\theta_w$. A look-up table for NLC drive specifications versus steering angle can be followed in this regard to avoid overlapped scanning zones. Similarly, in the final polarization state#16, the maximum steering angle (40.92°) is achieved with a value of $\theta_w$=0.199° which is less than the maximum value of $\theta_w$ as in this configuration of the scanner, any value of $\theta_w$ higher than 0.199° results in total internal reflection inside the last birefringent crystal prism. Hence, by controlling the polarization state and the NLC prism drive signals, a total steering angle of 40.92° can be obtained in the current configuration. For demonstration purposes, in Fig. 7, continuous scanning is shown between the final two polarization states (i.e., #15 & #16) since they constitute the worst case scenario where 7.12° of angular separation lies between these two spots.

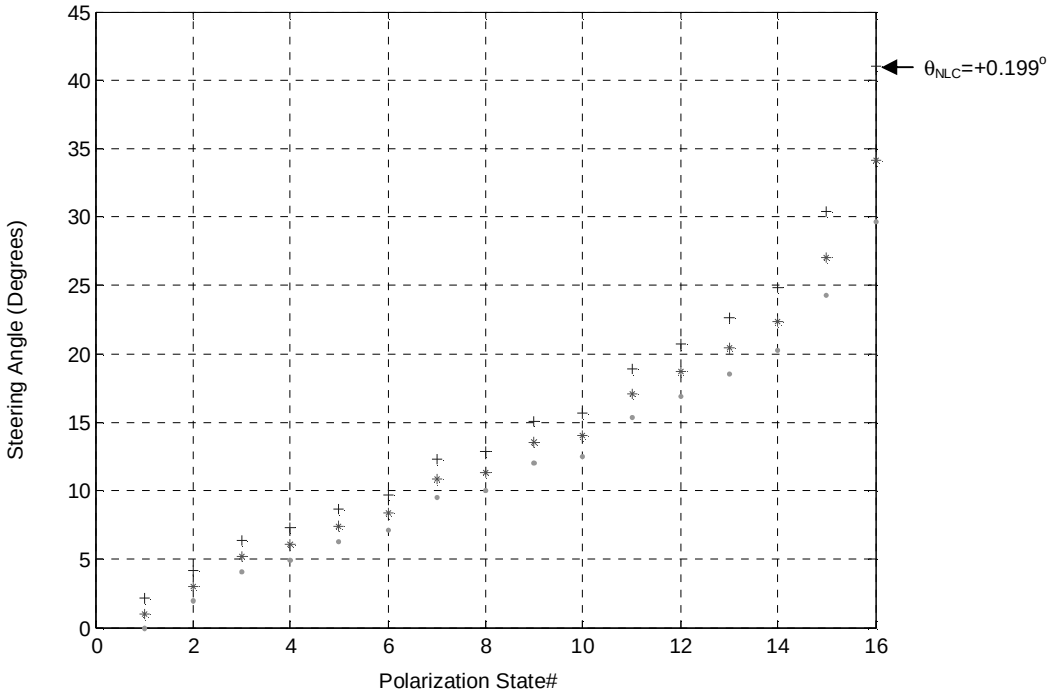


Fig. 6. Simulated steering angles for a 4-stage coarse and one stage fine 1-D digital P-MOS at 1550 nm that can continuously access any spot within a 40.92° wide scan domain. $\alpha_{NLC}$= ±0.35°, $\alpha_1$= –9.95°, $\alpha_2$= 19.95°, $\alpha_3$= 4.95° and $\alpha_4$ = 9.95° using Rutile prisms ($n_e$=2.454, $n_o$=2.71 @ $\lambda$=1550 nm).

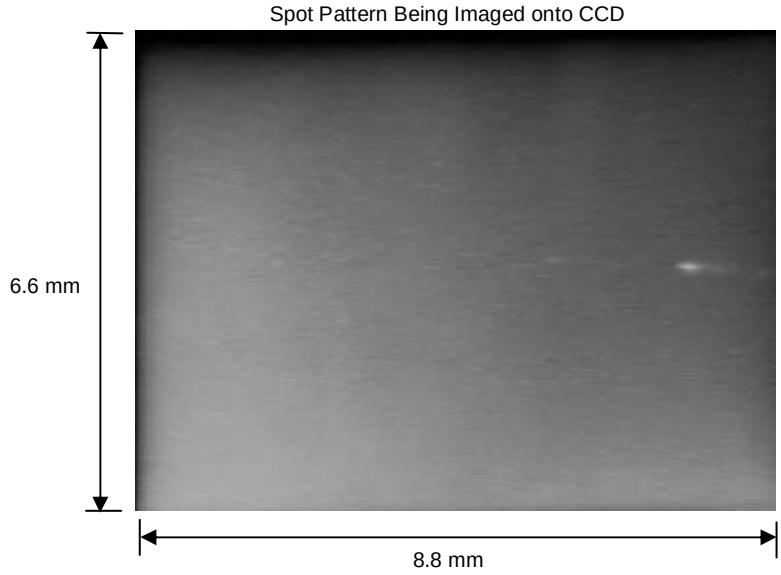


Fig. 7. Demonstration of continuous steering using NLC prism in the 4-stage coarse 1-D P-MOS scanner of Fig. 5. $\alpha_{NLC} = \pm 0.35^{o}$ (NLC: Merck BL006, $\Delta n = 0.229$ at 1550 nm and $25^{o}C$).

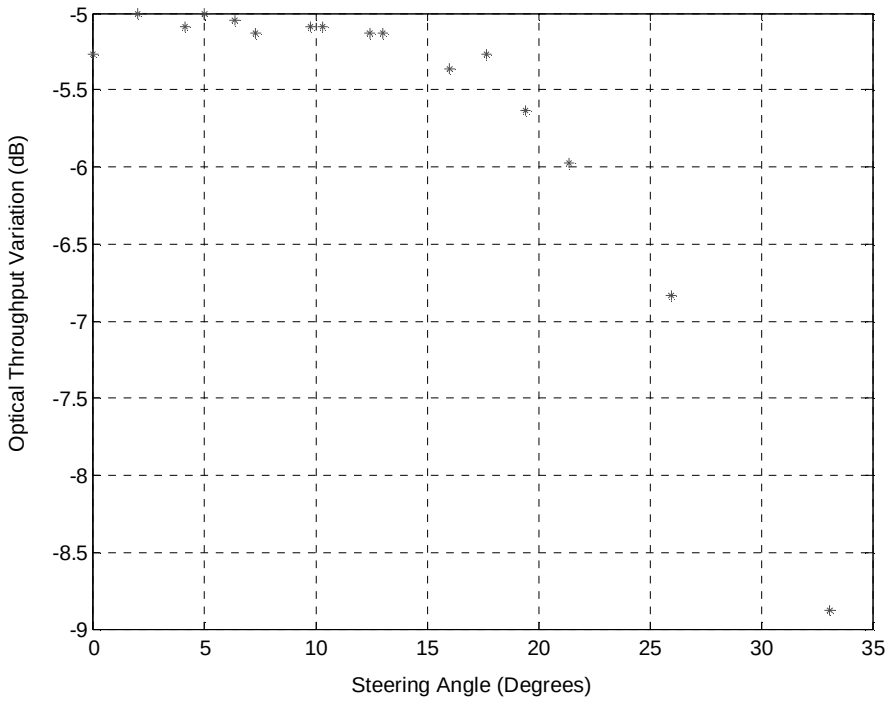


Fig. 8. Experimentally measured scanner optical throughput variation for the 4-stage 1-D coarse digital P-MOS demonstration at 1550 nm.

Throughput efficiency was measured for the far field spot pattern for the 16-point random scan (dataset * of Fig. 5) as shown in Fig. 8. It is observed that the throughput efficiency remains more or less constant in a broad angular range and decreases gradually as the steering angle reaches the maximum. The insertion loss for the experimental non-AR coated NLC prism was measured to be 0.73 dB which includes 0.35 dB loss from Fresnel reflections. The average insertion loss for the 1" diameter FLC PS's was measured to be 0.7 dB at 1550 nm while

their average optical polarization extinction ratio was 28 dB. The Rutile prisms had a 2 cm x 2 cm face area, were AR coated and had an average insertion loss of 0.04 dB. The insertion loss for these prisms varies as the angles of incidence and exit vary as shown by experimental data in Fig. 8. For the demonstrated 4-stage hybrid analog-digital P-MOS, the total average insertion loss is ~5 dB (=3*0.73 (For 3 NLCs) + 4*0.7 (For 4 FLC PSs)). This number is reduced to ~3.93 dB when a single AR coated NLC device is used instead of three NLC devices.

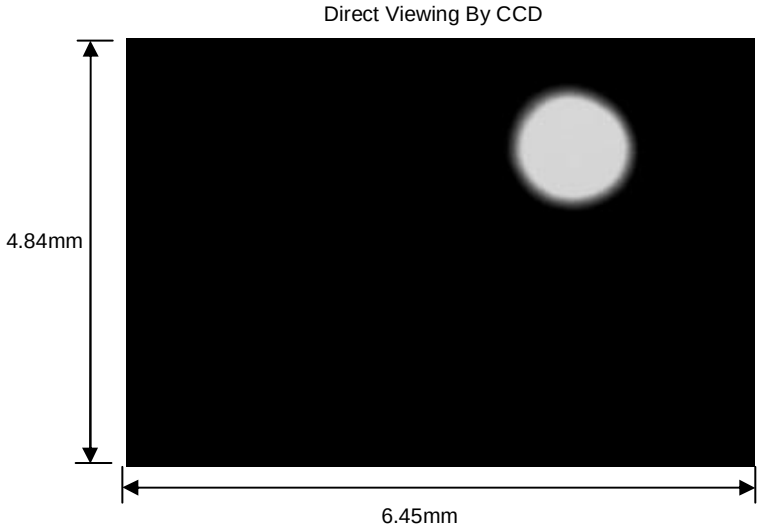


Fig. 9. Experimentally obtained 2-D far-field spot pattern for 2-stage coarse and 2-stage fine P-MOS demonstration at 1550 nm.

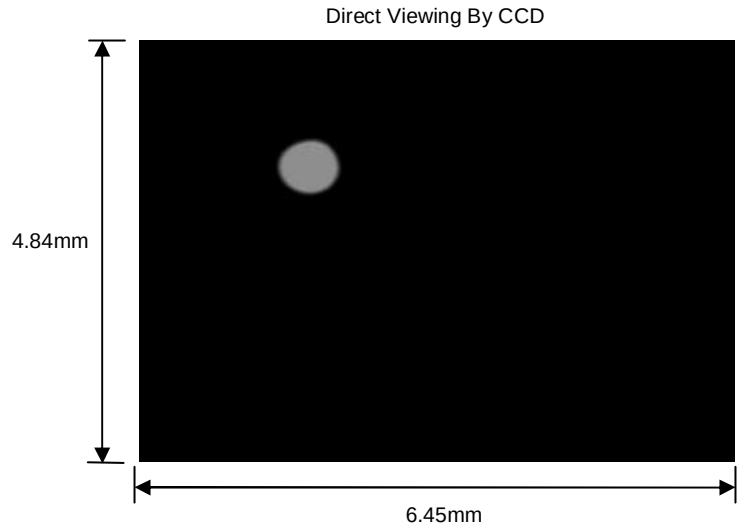


Fig. 10. Experimentally obtained 3-D spot pattern for 2-stage coarse and 3-stage fine P-MOS demonstration at 1550 nm.

Experiments were also carried out to demonstrate the capability of the P-MOS to steer the beam in two and three dimensions. Fig. 9 shows a 4-stage P-MOS, where two birefringent crystal prisms and two NLC prisms are used to digitally access 16-spot pattern (4-bit) in a two dimensional grid in the far-field. Recall that each stage has its own polarization switch. One birefringent crystal prism and an NLC prism are used to address each dimension. In the Fig. 10 demonstration, a 2-stage coarse and 3-stage fine P-MOS is used to address all three dimensions in a single scanner. The two coarse stages consist of birefringent crystal prisms while the three fine stages consist of two NLC prisms and a single NLC lens device.[19] The NLC lens is used to scan the third dimension; i.e., to focus or defocus the beam along its direction of propagation. The goal of this experiment was to demonstrate the capability of the P-MOS to scan all three dimensions in a desired fashion.

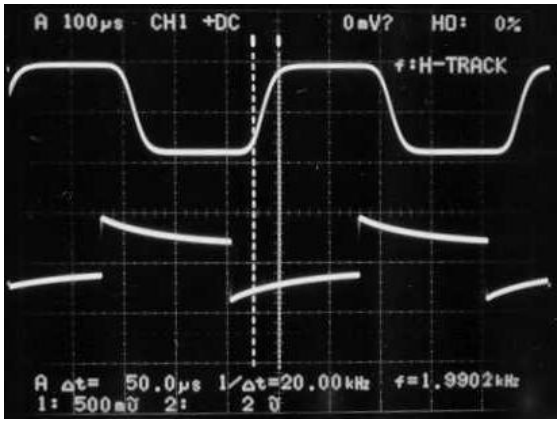


Fig. 11. Experimentally measured rise time for the FLC PS used in P-MOS demonstration at 1550 nm.

In the parallel drive P-MOS architecture, the scanner response time will depend upon the slowest device in the system. In a P-MOS where only birefringent crystal and fixed drive voltage LC prisms are used for scanning with actively driven FLC PSs, the scanner response time will be equal to a single FLC PS's response time. Figure 11 shows the measured 50 µsec fast response of the demonstrated FLC half wave plate at $\lambda$=1550 nm, alongwith the corresponding drive signal. Hence in the hybrid P-MOS where both birefringent crystal prisms and actively driven NLC prisms are used for scanning, the limiting factor for the response time is the NLC prism.

In order to get the relatively large NLC prism angles such as $0.35^o$ with a fast response time, multiple thin NLC cells can be cascaded in order to achieve the total angle of $0.35^o$. In this way, a scanning speed of the order of a few milliseconds can be achieved with the NLC device although at the expense of throughput efficiency. Today, research is being conducted in the area of high birefringence materials that have low viscosity.[28] Use of such materials will further reduce the response time of the NLC prism down into the sub-millisecond regime.

## 4. Conclusion

In summary, we have demonstrated a versatile polarization based scanner design that is well suited for optical beamforming applications such as freespace laser communications, 3-D displays, scanning 3-D optical microscopy, and data retrieval applications. Specifically, for the first time, 1550 nm band random as well as continuous mode large $40.92^o$ angle beam steering is experimentally demonstrated using a unique hybrid analog-digital mode P-MOS architecture that possesses high beam quality and minimal pixel-based high order diffractive effects. In particular, a unique electrical biasing control of the active NLC prism devices is used to provide a near continuous and high resolution beam scan over a wide angular dynamic range. Demonstrations include one, two and three dimensional beam steering experiments.

## Acknowledgments

This research is supported in part by the DARPA STAB program.

## References

1. U. J. Schmidt, "Optical processing of information," 1962 Proc. Washington Symposium, Eds. D. Pollock, C. Koester and J. Tippet, pages 98-103, Spartan, Washington, D.C, 1963.
2. W. Kulcke, T. Harris, K. Kosanke, E. Max, IBM J. Res. And Develop., **8**, pages 64-67, 1964.
3. T. Nelson, Bell Sys. Tech. J., **43**, pages 821-845, 1964.
4. W. Tabor, Bell Sys. Tech. J., **43**, pages 1153-1154, 1964.
5. U. J. Schmidt, "A high speed digital light beam deflector," Physics Letters, **12**, 3, 205-206, (Oct. 1964).

6. R. A. Soref, D. H. McMahon, "Optical design of Wollaston-prism digital light deflectors," Applied Optics, **5**, 3, 425-434, (Mar. 1966).
7. W. Kulcke, K. Kosanke, E. Max, M. A. Habegger, T. J. Harris, H. Fleisher, "Digital light deflectors," Applied Optics, **5**, 10, 1657-1667, (Oct. 1966).
8. V. J. Fowler, J. Schlafer, "A survey of laser beam deflection techniques," Applied Optics, **5**, 10, 1675-1682, (Oct. 1966).
9. T. C. Lee and J. D. Zook, "Light beam deflection with electrooptic prisms," IEEE Journal of Quantum Electronics, **4**, 7, 442-454, (Jul. 1968).
10. A. F. Fray and D. Jones, "Liquid crystal light deflector," U.S. Patent 4066334, (1978).
11. B. Lofving and S. Hard, "Beam steering with two ferroelectric liquid-crystal spatial light modulators," Opt. Lett. **23**, 19, 1541-1543, (1998).
12. M. H. Kiang, O. Solgaard, K. Y. Lau and R. S. Muller, "Electrostatic combdrive-actuated micromirrors for laser-beam scanning and positioning," Journal of Microelectromechanical Systems **7**, 1, 27-37, (1998).
13. R. A. Meyer, "Optical beam steering using a multichannel lithium tantalate crystal," Appl. Opt. **11**, 3, 613-616, (1972).
14. Q. W. Song, X. M. Wang, R. Bussjager and J. Osman, "Electro-optic beam-steering device based on a lanthanum-modified lead zirconate titanate ceramic wafer," Appl. Opt. **35**, 17, 3155-3162, (1996).
15. H. Meyer, D. Riekmann, K.P. Schmidt, U. J. Schmidt, M. Rahlff, E. Schroder and W. Thust, "Design and performance of a 20-stage digital light beam deflector," Appl. Opt. 11, 8, 1732-1736, (1972).
16. R. McRuer, L. R. McAdams and J. W. Goodman, "Ferroelectric liquid-crystal digital scanner," Opt. Lett., **15**, 23, 1415-1417, (1990).
17. C. M. Titus, P. J. Bos and O. D. Lavrentovich, "Efficient, accurate liquid crystal digital light deflector," Proc. SPIE, **3633**, 244, (1999).
18. N. A. Riza, "Digital control polarization based optical scanner," US Patent 6031658, (2000).
19. N. A. Riza and S. A. Khan, "Programmable High Speed Polarization Multiplexed Optical Scanner," Opt. Lett. **28**, 7, 561-563, (2003).
20. S. A. Khan and N. A. Riza, "Demonstration of 3-dimensional wide angle laser beam scanner using liquid crystals," Optics Express, **12**, 5, 868-882, (March 2004).
21. W. Klaus, "Development of LC optics for free-space laser communications," International Jounal of Electronic Communications **56**, 4, 243-253, (2002).
22. J. B. Hawthorn, A. Harwit, and M. Harwit, "Laser telemetry from space," Science, **297**, July 26, (2002).
23. B. W. Matkin, "Steered agile beams program support for Army requirements," Proc. SPIE, **4489**, 1-12, Free-Space Laser Communication and Laser Imaging; David G. Voelz, Jennifer C. Ricklin; Eds, 46th Annual Meeting of SPIE, 29 July - 3 August (2001).
24. P. Yeh and C. Gu, *Optics of Liquid Crystal Displays*, (John Wiley & Sons Inc., New York, 1999).
25. FLC Liquid Crystal Light Valves User Manual, Displaytech Inc., Longmont, CO, USA, (1996).
26. M. Yu. Loktev, V. N. Belopukhov, F. L. Vladimirov, G. V. Vdovin, G. D. Love and A. F. Naumov, "Wave front control systems based on modal liquid crystal lenses," Review of Scientific Instruments **71**, Issue 9, 3290-3297, September (2000).
27. N. A. Riza and M. C. DeJule, "Three-terminal adaptive nematic liquid-crystal lens device," Opt. Lett. **19**, Issue 14, 1013-1015, (1994).
28. S. Gauza, H. Wang, C. H. Wen, S. T. Wu, A. Seed, and R. Dabrowski, "High Birefringence Isothiocyanato Tolane Liquid Crystals," Japanese Journal of Applied Physics Part I, **42**, 3463-3466, (2003).